Displacement-length scaling relations for faults on the terrestrial planets

Richard A. Schultz[*], Chris H. Okubo[1], Scott J. Wilkins[2]

Geomechanics-Rock Fracture Group, Department of Geological Sciences and Engineering/172, University of Nevada, Reno, NV 89557-0138, USA

Abstract

Displacement-length (D/L) scaling relations for normal and thrust faults from Mars, and thrust faults from Mercury, for which sufficiently accurate measurements are available, are consistently smaller than terrestrial D/L ratios by a factor of about 5, regardless of fault type (i.e. normal or thrust). We demonstrate that D/L ratios for faults scale, to first order, with planetary gravity. In particular, confining pressure modulates: (1) the magnitude of shear driving stress on the fault; (2) the shear yield strength of near-tip rock; and (3) the Young's (or shear) modulus of crustal rock. In general, all three factors decrease with gravity for the same rock type and pore-pressure state (e.g. wet conditions). Faults on planets with lower surface gravities, such as Mars and Mercury, demonstrate systematically smaller D/L ratios than faults on larger planets, such as Earth. Smaller D/L ratios of faults on Venus and the Moon are predicted by this approach, and we infer still smaller values of D/L ratio for faults on icy satellites in the outer solar system. Collection of additional displacement-length and down-dip height data from terrestrial normal, strike-slip, and thrust faults, located within fold-and-thrust belts, plate margins, and continental interiors, is required to evaluate the influence of fault shape and progressive deformation on the scaling relations for faults from Earth and elsewhere.
© 2006 Elsevier Ltd. All rights reserved.

Keywords: Displacement-length scaling; Faulting; Tectonics; Mars

1. Introduction and background

Populations of faults on planetary surfaces (beyond the Earth) provide an informative and additional suite of datasets for use by structural geologists (see review and discussion by Schultz, 1999). The lack of significant atmosphere on Mercury, the Moon, and most icy satellites, combined with exceedingly slow erosion rates (associated with an absence of fluvial, pluvial, eolian, and hydrologic processes), permits preservation of unusually clear fault morphologies. Given a lack of crustal recycling and Earth-like plate tectonics on most planetary bodies, such as Mars, a visible record of single or superposed faulting episodes may be preserved, revealing details of the development of the fault populations over several orders of magnitude of length. As a result, planetary surfaces provide unique natural laboratories for studying the process of faulting under a wider range of environmental conditions (gravity, pore-water pressure, temperature, tectonic regime) than is possible by using terrestrial fault sets alone.

Faults have been documented on nearly every geologic surface in the solar system and a vast literature exists on the subject of planetary structural geology. Normal fault and graben systems are probably the most common, accommodating both localized and distributed extension on Mercury, Venus, the Moon, Mars, Europa, Ganymede, and several smaller icy satellites of the outer planets including Tethys, Dione, and Miranda. Thrust faults have been identified on Mercury, Venus, the Moon, and Mars. Strike-slip faults have been identified on Mars (e.g. Schultz, 1989, 1999; Okubo and Schultz, 2006) and on some icy satellites although large lateral displacements such as those found systematically at terrestrial transform plate boundaries are currently recognized only on

* Corresponding author.
  E-mail addresses: schultz@mines.unr.edu (R.A. Schultz), chriso@pirl.lpl.arizona.edu (C.H. Okubo), scott.wilkins@shell.com (S.J. Wilkins).
[1] Present address: Lunar and Planetary Laboratory, The University of Arizona, Tucson, AZ 85721-0063, USA.
[2] Present address: Shell International Exploration and Production, Inc., Bellaire Technology Center, P.O. Box 481, Houston, TX 77001, USA.

Europa. At present the resolution of orbital spacecraft imaging systems is insufficient to resolve individual dilatant cracks (joints), although subsurface igneous dikes have recently been inferred on Mars from surface topographic data (Schultz et al., 2004).

Precision measurements of the maximum displacement, D_{max} and map lengths (L) of surface-breaking faults on Mars (Schultz, 1997; Wilkins et al., 2002; Watters, 2003; Hauber and Kronberg, 2005) and Mercury (Watters et al., 1998, 2000, 2002) demonstrate that less displacement per unit length is accumulated along faults on these planets than along terrestrial (Earth-based) ones. For example, normal faults from Tempe Terra (Mars) and thrust faults from Arabia (Mars) show ratios of maximum displacement to length $D/L=\gamma=6.7\times10^{-3}$ (Wilkins et al., 2002) and 6×10^{-3} (Watters et al., 1998), respectively. Thrust faults from Mercury also show D/L ratios of 6.5×10^{-3} (Watters et al., 2000, 2002). Typical values for terrestrial faults (normal, strike-slip, or thrust) are $\sim1-5\times10^{-2}$ (e.g. see compilations and discussions by Cowie and Scholz (1992a), Clark and Cox (1996), Schlische et al. (1996), Schultz and Fossen (2002) and Davis et al. (2005)). Currently, topographic data of sufficient accuracy and resolution to assess displacement-length ($D-L$) scaling of non-terrestrial faults are available only for Mars and Mercury.

In this paper we demonstrate the key role played by a planet's surface gravitational acceleration ('gravity' in this paper) in $D-L$ scaling of faults. We incorporate gravity explicitly into updated $D-L$ scaling relations for faults (following Cowie and Scholz (1992b) and Schultz and Fossen (2002)). We show that the systematic shift toward smaller maximum displacements for normal and thrust faults on Mars and Mercury is related to the reduced gravity on these planets relative to the Earth.

2. D-L scaling of faults

Data from the literature for normal faults from Earth and Mars are shown in Fig. 1. The data for Martian normal faults are systematically shifted to smaller values of displacement by a factor of about 5 from the terrestrial data. A similar downward shift is evident for thrust faults on both Mars and Mercury (see discussion below). Measurements of Martian fault displacements (i.e. topographic offset corrected by fault dip angle) have uncertainties of a few meters or less, whereas those for Mercury have uncertainties in the topography of perhaps tens of meters (e.g. Watters et al., 2000). Detailed examination of Martian and Mercurian faults indicates that the smaller D/L ratios result from smaller displacements (e.g. Watters et al., 1998, 2000, 2002; Wilkins et al., 2002); an overestimation of fault lengths by the same factor of 5 is not likely based on clearly resolved fault traces (e.g. Schultz and Fori, 1996; Wilkins and Schultz, 2003).

2.1. Why should fault displacements scale with gravity?

In this section we derive an expression that reveals the dependence of the $D-L$ scaling relations for faults on planetary
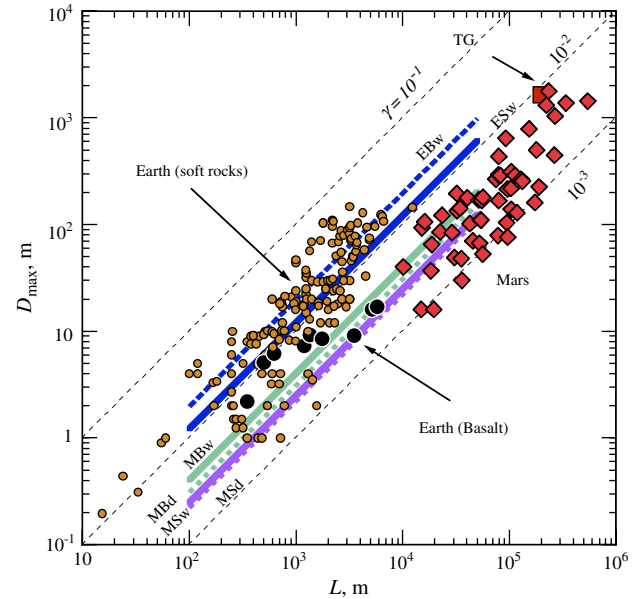

Fig. 1. $D-L$ data for normal faults from Earth (gray circles, sandstone and non-welded tuff; black circles, basalt) and Mars (gray diamonds, Tempe Terra; gray square, Thaumasia graben, linked faults, 'TG'); data from Schlische et al. (1996), Wilkins et al. (2002), and Hauber and Kronberg (2005). Calculated scaling relations (Eq. (9); see text for parameters): EBw, Earth basaltic rock mass with wet conditions; ESw, Earth sandstone rock mass with wet conditions; MBw, Mars basaltic rock mass with wet conditions; MBd, Mars basaltic rock mass with dry conditions; MSw, Mars sandstone rock mass with wet conditions; MSd, Mars sandstone rock mass with dry conditions.

gravity. The analysis in this section applies to all three types of faults (normal, thrust, and strike-slip). For the case of normal faulting, for example, the stress difference ($\sigma_1-\sigma_3$ or $\sigma_v-\sigma_h$) is proportional to the shear driving stress σ_d (Schultz, 2003; see Table 1 for explanation of variables used in this paper). Substituting the Hooke's law relations for three-dimensional strain (e.g. Jaeger and Cook, 1979) for the stress difference shows that

$$\sigma_d = \frac{E}{(1+\nu)}(\epsilon_v - \epsilon_h), \qquad (1)$$

Where E and ν are the Young's modulus and Poisson's ratio respectively, of the faulted

The crustal strain difference ($\epsilon_v-\epsilon_h$) can be rewritten using the far-field stress state, rather than the shear driving stress on an individual dipping fault, by noting that $\sigma_v=q\sigma_h$, with q related to the maximum (static) friction coefficient on the faults ($\sqrt{\mu^2+1}+\mu^2)^2$ (Jaeger and Cook, 1979, p. 97; McGarr and Gay, 1978; Brace and Kohlstedt, 1980; Zoback et al., 2003) as

$$(\epsilon_v - \epsilon_h) = \frac{(1+\nu)}{E}\left(\frac{q-1}{q}\right)\rho g z \qquad (2)$$

where ρ is average (wet or dry) rock density, g is gravity, and z is depth.

Using the relationship between crustal strains and the geometric moments of a fault population and assuming 'small faults' for simplicity (i.e. faults with down-dip heights less

Table 1
Main variables and parameters used in displacement-length scaling calculations

Section	Symbol	Explanation and units
Scaling from crustal strains		
	e_v	Vertical elastic normal strain
	e_h	Minimum horizontal elastic normal strain
	V	Volume of faulted crustal section, m^3
	κ	Ratio of average to maximum displacement on fault
Fault slip		
	τ	Shear stress resolved on fault plane, MPa
	σ_n	Normal stress resolved on fault plane, MPa
	σ_1	Maximum compressive remote principal stress, MPa
	σ_3	Minimum compressive remote principal stress, MPa
	σ_v	Vertical compressive remote principal stress, MPa
	σ_h	Minimum horizontal compressive remote principal stress, MPa
	σ_H	Maximum horizontal compressive remote principal stress, MPa
	ρ	Crustal rock density, kg m^{-3}
	g	Gravitational acceleration at planetary surface, m s^{-2}
	z	Depth below planetary surface, m
	δ	Fault dip angle, degrees
	ϕ	Fault dip parameter, degrees
	μ	Coefficient of friction used with local (fault-centered) stress state
	μ_s	Maximum ('static') friction coefficient for fault slip increment
	μ_d	Minimum ('dynamic') friction coefficient for fault slip increment
	$\Delta\mu$	Friction difference for driving stress calculation
	q	Friction parameter used with remote stress state
Displacement-length scaling		
	D_{max}	Maximum displacement (structural offset) along fault plane, m
	L	Horizontal fault length, m
	H	Vertical fault height measured in fault plane, m
	γ	Ratio of D_{max}/L
	n	Exponent of displacement-length scaling law
	D	Abbreviated (colloquial) form of D_{max}, m
	E	Young's modulus of rock surrounding the fault, GPa
	ν	Poisson's ratio of rock surrounding the fault
	σ_d	Shear driving stress on fault ($=\Delta\mu\sigma_n$), MPa
	σ_y	Shear yield strength of rock mass at the fault tip, MPa
	C	Variable or function that removes near-tip singularity
	L/H	Fault aspect ratio
	a	Half-length of fault, m
	b	Half-height of fault, m
	N	Scaling parameter, ratio of cumulative to incremental displacement
Yield strength		
	RMR	Rock mass rating
	σ_c	Unconfined compressive strength of intact rock material, MPa
	m_i	Hoek−Brown parameter characterizing intact rock material
	m	Hoek−Brown parameter characterizing rock mass texture
	s	Hoek−Brown parameter characterizing rock mass fracturing
Modulus		
	S	Stiffness of rock mass, GPa^{-1}
	E^*	Deformation modulus, GPa

than the thickness of an enclosing brittle layer; e.g. Scholz, 1997; Schultz, 2003)

$$\epsilon_v = -\frac{\sin(\delta)\cos(\delta)}{V}\sum_{i=1}^{N}(DLH)_i$$

$$\epsilon_h = \frac{\kappa\gamma\sin(\delta)\cos(\delta)}{V}\sum_{i=1}^{N}(L^2H)_i \qquad (3)$$

where κ is the ratio of average displacement on the fault to its maximum displacement, with typical values of 0.6−0.7, V is the volume of the faulted layer, H is the down-dip fault height and δ is the fault dip angle. For the representative case of a single fault (to illustrate the results most clearly), we find that

$$(\epsilon_v - \epsilon_h) = -L^2H\left(\frac{\gamma\sin(\delta)\cos(\delta)}{V}\right)(1+\kappa) \qquad (4)$$

Substituting $(LDH)/\gamma$ for L^2H in Eq. (4) and solving for fault displacement yields

$$D = \frac{(1+\nu)}{E}\left(\frac{q-1}{q}\right)\left(\frac{\rho gz}{LH(1+\kappa)}\right)\left(\frac{V}{\sin(\delta)\cos(\delta)}\right) \qquad (5)$$

Eq. (5) reveals that the magnitude of maximum displacement D on a normal, strike-slip, or thrust fault scales with planetary gravity g, for constant values of fault shape (κ, L, H, δ), crustal rock properties (E, ν, ρ), and size of the deforming domain (z, V). This relation demonstrates the physical basis for the scaling relations implied by the data shown in Fig. 1 and motivates the more detailed analysis presented in the next section.

2.2. Mechanical models of faults

In order to investigate the effect of different planetary gravities on fault displacements, and thereby to D/L ratios, we consider one member of a class of mechanical models for faults that is consistent with linear D-L scaling (Scholz, 2002, p. 116), finite rock (yield) strength at the tipline (Cowie and Scholz, 1992b; Scholz, 1997), and gentle near-tip displacement gradients (e.g. Cowie and Scholz, 1992b; Bürgmann et al., 1994; Moore and Schultz, 1999; Cooke, 1997; Cowie and Shipton, 1998). Called variously 'post-yield' or elastic-plastic fracture mechanics models depending on their particular approaches, these models specify a yield strength on the same order (e.g. MPa) as the driving stress, considerably smaller than that implicitly assumed in linear elastic fracture mechanics (LEFM) models of faults (e.g. Pollard and Segall, 1987).

Two important members of this class of models are the 'end-zone' model (e.g. Cowie and Scholz, 1992b; Bürgmann et al., 1994; Cooke, 1997; Martel, 1997; Willemse and Pollard, 1998; Schultz and Fossen, 2002; Wilkins and Schultz, 2005) and the 'symmetric linear stress distribution' model (Bürgmann et al., 1994). We use the 'end-zone' model in this paper for an individual fault having a central well-slipped portion bounded by frictionally stronger end zones. The other

end-member that assumes a linear increase in fault frictional strength, from the center to the tip (Bürgmann et al., 1994), produces a nearly linear displacement distribution as demonstrated by measurements for many faults (e.g. Dawers et al., 1993; Cowie and Shipton, 1998; Manighetti et al., 2001; Soliva and Benedicto, 2004). The governing factors as evaluated in this paper are the same in either case. We are not aware of any observations that would suggest a planet-dependent model of fault displacement, so we use a single model for consistency across all planetary bodies considered. The particular choice of post-yield fault model is thus not critical to the scaling conclusions drawn in this paper. The variables and parameters used in this analysis are given in Table 1.

The general form of this class of models is

$$\frac{D_{max}}{L} = \frac{2(1-\nu^2)}{E}(\sigma_d - C\sigma_y) \qquad (6)$$

in which D_{max} is the (maximum) shearing displacement located at the fault midpoint (referred to as D in this paper), L is horizontal fault length, σ_d is the shear driving stress (Cowie and Scholz, 1992b; Gupta and Scholz, 2000a; Schultz, 2003; see Table 1), σ_y is the yield strength of rock at the fault tip, and C is a variable (or function) that specifies how the theoretical stress singularity at the fault tip is removed; specifically,

$$C = 1 - \cos\left(\frac{\pi}{2}\frac{\sigma_d}{\sigma_y}\right) \qquad (7a)$$

(End-zone model; Schultz and Fossen, 2002)

$$C = 1/\pi \qquad (7b)$$

(Linear displacement model; Bürgmann et al., 1994)

The cosine term in Eq. (7a) defines the length of the end zone (s/a in Eq. (7b) of Schultz and Fossen, 2002) adjoining the fully slipped central part of a fault. C in Eq. (7b) is obtained by setting $x/a=0$ and $L=2a$ in Eq. (14) of Bürgmann et al. (1994), with their quantities S_r and S_g being interpreted as σ_d and σ_y, respectively (S. Martel, personal communication, 2004). The LEFM solution, with its inherent singularity in near-tip stress and the associated elliptical displacement profile, is recovered by setting $C=0$ in Eq. (6). Eq. (6) is comparable with that obtained by Scholz (1997) in his discussion of end-zone models and D-L scaling relations.

Eq. (6) has several important and useful properties. First, the effective stress drop on the fault ($\sigma_d - C\sigma_y$) is independent of fault length. Second, the D/L ratio depends explicitly (and linearly) on the driving stress, rock properties, and yield strength. As a result, this *class of models* provides a physical basis for D-L scaling relations of the form $D=\gamma L$ (e.g. Cowie and Scholz, 1992a; Clark and Cox, 1996; Schultz and Fossen, 2002; Scholz, 2002, p. 116).

Using the end-zone model, the D-L relationship for a fault of variable map length $L=2a$ and down-dip height $H=2b$ is given by (Schultz and Fossen, 2002)

$$\frac{D_{max}}{L} = \frac{2(1-\nu^2)}{E}N\frac{\left\{\sigma_d - \sigma_y\left[1-\cos\left(\frac{\pi\sigma_d}{2\sigma_y}\right)\right]\right\}}{\sqrt{1+1.464\left(\frac{a}{b}\right)^{1.65}}} \qquad (8)$$

in which N is a scaling parameter related to the ratio of cumulative to incremental displacements (Schultz, 2003). Plausible values of σ_y/σ_d appear to be approximately 2–3 (e.g. Cowie and Scholz, 1992b; Schultz and Fossen, 2002; Wilkins and Schultz, 2005). Three-dimensional faults having more nearly triangular displacement distributions (e.g. Dawers et al., 1993; Cowie and Shipton, 1998; Manighetti et al., 2001; Soliva and Benedicto, 2004) can be considered, in part, by rewriting Eq. (8) with Eq. (7b) instead of Eq. (7a) in the numerator (Schultz and Soliva, 2005).

Terrestrial dip-slip faults appear to have roughly elliptically shaped fault planes, with aspect ratios (L/H) of 2–3 (Nicol et al., 1996). For faults having a constant aspect ratio of $L/H=3$, Eq. (8) simplifies to become

$$\frac{D_{max}}{L} = \frac{2(1-\nu^2)}{E}\frac{N}{3.16}\left\{\sigma_d - \sigma_y\left[1-\cos\left(\frac{\pi\sigma_d}{2\sigma_y}\right)\right]\right\} \qquad (9)$$

For faults with an aspect ratio of 2 (half-length equals depth for surface-breaking faults), the geometry term in the denominator of Eq. (9) would equal 2.37 instead of 3.16.

Although aspect ratios may change for faults over their length scales (e.g. Willemse et al., 1996; Willemse, 1997; Schultz and Fossen, 2002; Soliva et al., 2005) or between populations, we choose to hold this parameter constant ($L/H=3$) in this analysis to minimize the number of variables (but see discussion of thrust fault data below). We know of no basis to speculate that aspect ratios should differ systematically for isolated, unlinked faults on different planetary bodies, although some evidence suggests vertical restriction of some normal faults on one part of Mars to near-surface layers (Schultz, 2000a, 2003; Polit et al., 2005a,b). As shown by Nicol et al. (1996), Gupta and Scholz (2000b), Wilkins and Gross (2002), and Soliva et al. (2005, 2006), for example, restricted faults can be identified once fault lengths, displacements, layer thickness and/or spacing are known.

3. D-L scaling of faults

Eq. (6) shows that the D/L ratio for faults depends on three primary factors: modulus, shear driving stress, and yield strength. As shown above by Eq. (5), all three factors are influenced to various degrees by planetary gravity g. In this section we evaluate each of these factors and calculate the scaling relations for faults on Mars, Mercury, and the Moon.

3.1. Driving stress

This is the shear stress leading to Coulomb frictional sliding and attendant displacement along the fault. The relations for Coulomb frictional sliding ($|\tau|=\sigma_n\Delta\mu$) can be rewritten

using the remote principal stresses (e.g. Jaeger and Cook, 1979, pp. 95−96), noting that the right-hand side of the Coulomb relation $(\sigma_n \Delta \mu)$, $\{[(\sigma_1+\sigma_3)/2]-[(\sigma_1-\sigma_3)/2]\sin 2\phi\}\Delta\mu$, represents the shear driving stress σ_d (Schultz, 2003), $\Delta\mu$ is the difference between static and dynamic friction coefficients for single-slip events (Cowie and Scholz, 1992b; Cooke, 1997; Scholz, 1998; Schultz, 2003; see discussion below), ϕ is either the fault dip δ (for thrust faults), or $(90°-\delta)$ (for normal faults), τ is shear stress resolved on the fault plane, and σ_n is the magnitude of effective (compressive) normal stress resolved from remote tectonic stresses onto the fault plane. Normal faulting implies a vertical maximum principal stress $\sigma_v = \rho g z$, with depth z set equal to 100 m for this analysis, and a least horizontal principal stress $\sigma_h = \sigma_v/q$. For faults, the relevant quantity is the cumulative shear driving stress (Cowie and Scholz, 1992b; Gupta and Scholz, 2000a; Schultz, 2003) associated with the total (cumulative) geologic offset along the fault (invoked through multiplication of in-situ stress by N). We choose values for the static and dynamic coefficients of friction of $\mu_s = 0.6$ and $\mu_d = 0.59$ (e.g. Marone, 1998; Scholz, 1998; Schultz, 2003) to calculate the shear driving stress. These parameters imply similar values of slip rates and seismic recurrence intervals on the faults.

The shear driving stress is reduced on lower gravity planets because the resolved effective normal stress σ_n, and the horizontal and vertical far-field stresses (which promote fault slip), are all dependent on σ_v and therefore on g. Previous modeling of fault-related topography on Mars (Schultz and Lin, 2001; Schultz and Watters, 2001; Wilkins and Schultz, 2003; Schultz et al., 2004) and Mercury (Watters et al., 2000, 2002), and some measurements (using older low-precision data for Martian faults: Davis and Golombek, 1990), show that fault dip angles, and hence values of friction (see also Neuffer and Schultz, in press), are similar to first order for all three planets.

3.2. Yield strength

The shear yield strength of unfaulted rock at the fault's tipline σ_y modulates the D/L ratio (e.g. Bürgmann et al., 1994; Cooke, 1997; Martel, 1999; Wibberley et al., 1999, 2000). Stronger rock requires greater near-tip stresses to break, leading to larger values of displacement along the fault (Cowie and Scholz, 1992b; Wibberley et al., 1999, 2000; Schultz and Fossen, 2002; Wilkins and Gross, 2002).

Rock strength is calculated from the Hoek−Brown (Mohr) envelope for rock masses (Hoek and Brown, 1980), which is a nonlinear Mohr envelope that includes the contributions to shear strength of joints and other fractures, lithology, scale, and pore-water conditions (see Schultz (1996) and Okubo and Schultz (2004) for detailed discussions and applications to structural geology). We assume a rock mass rating (RMR) of 50, appropriate for wet conditions (i.e. hydrostatic pore-pressure) and typical near-surface fracture densities (e.g. Bieniawski, 1989); dry conditions are considered by increasing RMR to 65, following standard practice (e.g. Bieniawski, 1989). For the basalt, $\rho = 2900$ kg m^{-3}, $m_i = 22$, and the

unconfined compressive strength of the intact rock material $\sigma_c = 250$ MPa; for a weaker rock mass (such as tuff or poorly indurated sedimentary material), the parameters for sandstone are used ($\rho = 2200$ kg m^{-3}, $m_i = 19$, $\sigma_c = 100$ MPa).

The yield strength is taken to be the peak shear strength (or maximum differential stress, equal to $\sigma_1 - \sigma_3$, or $\sigma_v - \sigma_h$ in a normal faulting environment and $\sigma_H - \sigma_v$ for thrust faulting) of the rock mass (where σ_h is the minimum horizontal compressive stress and σ_H is the maximum horizontal compressive stress). Mohr envelopes for strong (basalt) and weak (tuff or sandstone) rock masses on Earth and Mars are calculated and shown for equal depths of 1 km in Fig. 2. Because the σ_v increases with g, so does the diameter $(\sigma_1 - \sigma_3)$ of the Mohr circle and, in turn, the peak strength of the rock mass at any given depth. *Rock strength increases with planetary gravity for the same depth range below the surface* and is analogous to the well-known dependence of peak strength and confining pressure observed in experiments.

3.3. Modulus

The Young's modulus of crustal rock is included in the stiffness term S in Eq. (6), given by $S \propto (1-\nu^2)/E$. The various moduli (Young's, shear, and deformation; Bieniawski, 1989; Schultz, 1996) are interchangeable in this equations. As the modulus increases, displacement (and D_{max}) along a fault decreases (e.g. Wibberley et al., 1999, 2000).

Young's modulus is given by a value at the surface corresponding to the deformation modulus (Bieniawski, 1989; Schultz, 1996), which then increases with depth (e.g. Rubin, 1990). Deformation modulus is the field-scale equivalent of Young's modulus that includes the softening effects of joints and ground water. It is obtained from RMR by using Eq. (11) below (Bieniawski, 1989, p. 64; Schultz, 1996). The increase in modulus with depth results from the combined effect of mechanical compaction and the associated reduction in pore space with an increasing overburden, and diagenesis and cementation that occur in response to increasing temperatures. Because density and the pore-pressure state of the crust (that both modulate E) depend on confining pressure, *Young's modulus decreases with gravity for equivalent conditions and depth ranges below the surface*. For the Earth, assuming hydrostatic (wet) pore-water conditions and a basaltic rock mass (Rubin, 1990), the values of Young's (or shear) modulus are closely fit by

$$E = E^* + z^{0.4} \tag{10}$$

where E^* is the deformation modulus given by

$$E^* = 10^{\left(\frac{RMR-10}{40}\right)} \tag{11}$$

We calculate Young's modulus vs. depth on other terrestrial (i.e. rocky) planets by specifying the pore-water state (wet or dry), rock type, and planetary gravity. Shear modulus in the crust is proportional to the P-wave velocity (V_p) squared times
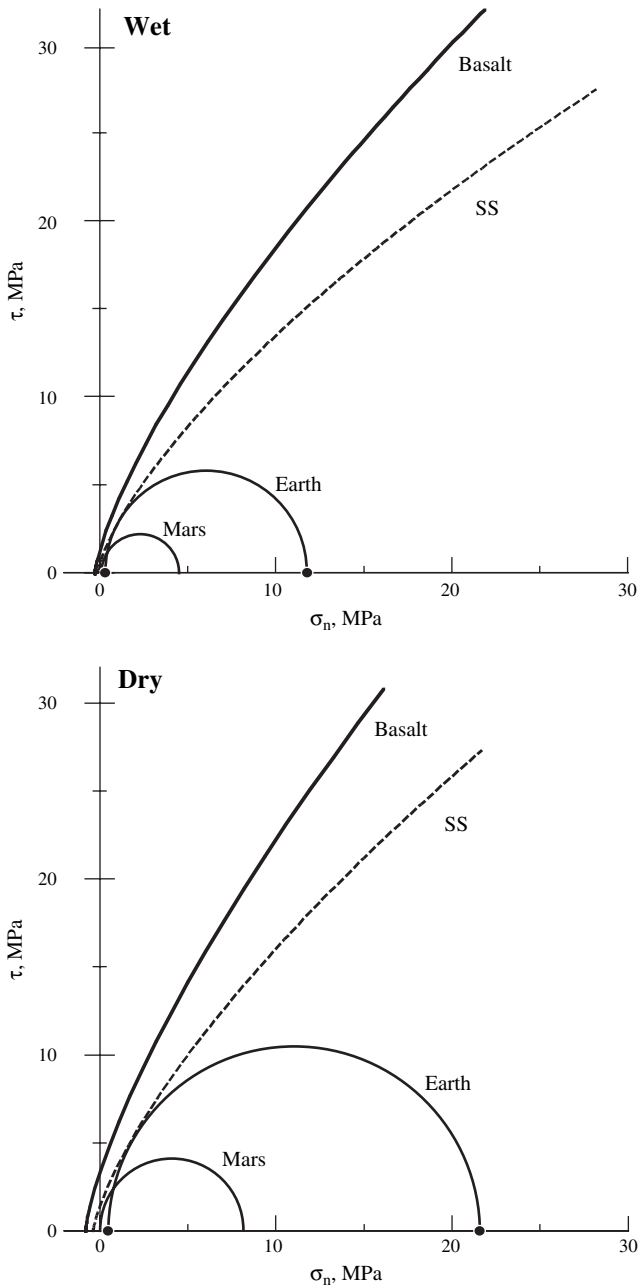
Fig. 2. Effect of planetary gravity on near-tip yield strength. Upper panel, water-saturated (wet) crustal rock; lower panel, anhydrous (dry) rock; Mohr circles for Earth and Mars shown for normal faulting regime at $z=1$ km. Yield strength curves calculated using Hoek–Brown relations for wet basalt (RMR=50, $m_i=22$, $\sigma_c=250$ MPa, wet rock density $\rho=1900$ kg m^{-3}), wet sandstone (RMR=50, $m_i=19$, $\sigma_c=100$ MPa, wet rock density $\rho=1200$ kg m^{-3}), dry basalt (RMR=65, $m_i=22$, $\sigma_c=250$ MPa, dry rock density $\rho=2900$ kg m^{-3}), and dry sandstone (RMR=65, $m_i=19$, $\sigma_c=100$ MPa, dry rock density $\rho=2200$ kg m^{-3}).

rock density (Bolt, 1988, p. 31; Rubin, 1990), with Young's modulus related to the shear modulus by standard relationships (Jaeger and Cook, 1979). Differences in these two conditions on other terrestrial planets are considered by scaling the density of crustal rocks (wet or dry) to the terrestrial reference case (Eq. (10)) that assumes wet basalt using

$$E = E^* + \left(\frac{g}{g_{Earth}}\right)\left(\frac{\rho}{\rho_{Earth}}\right)z^{0.4} \qquad (12)$$

The normalized gravity term in Eq. (12) adjusts V_p, whereas the normalized density term accounts for the pore-water state and rock type of the terrestrial planet's crust. Fractures and microcracks in the crusts of smaller planets will remain open to greater depths than for Earth, assuming constant rock type and pore-water conditions, leading to smaller values of modulus at any given depth.

Representative curves of Young's modulus vs. depth for Earth and Mars are shown in Fig. 3. Young's modulus for water-saturated Martian basaltic crust has the same value of deformation modulus as for the Earth ($E^*=10$ GPa, calculated from RMR=50) but increases at a slower rate with depth due to the reduced Martian gravity. A Martian rock mass containing water ice within the fracture porosity (Okubo and Schultz, 2004) has a strength that is closer to the water-saturated one than to the dry one. On the other hand, Young's modulus for dry Martian basaltic crust ($E^*=23.7$ GPa) is greater than that for the wet terrestrial case, with a larger deformation modulus at the surface associated with a dry rock mass (RMR=65) and a gradient ~10% larger than the wet terrestrial one. The variation in Young's modulus with depth for the dry Martian case is nearly the same as for dry Mercurian crust; the curves for Venus and the Moon are readily calculated from Eq. (12) by using dry rock densities and appropriate values of g.

4. Application to planetary bodies with different surface gravities

Planetary gravity enters into each of the three factors discussed above (Eq. (6)), but more subtly than simply as a ratio of planetary gravities (e.g. g_{Mars}/g_{Earth}) because the total reduction in D/L for a planetary fault population exceeds the gravity ratio (Fig. 1). Although driving stress scales directly
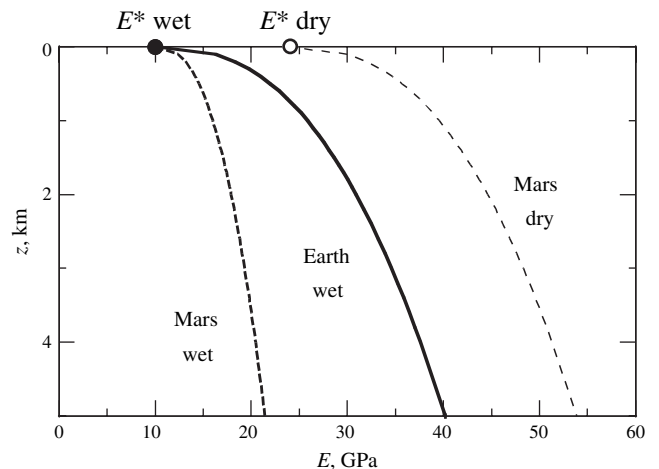

Fig. 3. Effect of planetary gravity on crustal deformability (Young's modulus) calculated by using Eq. (12). E^*, deformation modulus at $z=0$ km, calculated from Rock Mass Rating (RMR) by using Eq. (11).

with gravity, other factors including crustal density, pore-water content, and nonlinearity in the rock-mass yield strength envelope also affect the ratio in detail (see Section 2).

Displacements along terrestrial faults of a particular population have been demonstrated statistically (Cowie and Scholz, 1992a; Clark and Cox, 1996) to scale linearly with their length, so that $D_{max}=\gamma L^n$, with $n=1$. We find that linear scaling (with $n=1$) giving a constant ratio of D/L as on Fig. 1; Cowie and Scholz, 1992a; Clark and Cox, 1996) requires that constant values of shear driving stress, rock (yield) strength, aspect ratio (Schultz and Fossen, 2002; Soliva et al., 2005), and modulus must be maintained across the length scale of the fault population. For example, incorporating larger values of modulus, driving stress, and yield strength for larger (and thus, deeper) faults (all three averaged over the appropriate depth of faulting) leads to a steeper slope on the D/L plot of $n=1.8$. This result is in accord with previous suggestions (e.g. Cowie and Scholz, 1992a) that longer faults cut 'stronger rock' and hence should show larger displacements. Our calculations suggest, however, that the steeper slope results because the shear driving stress increases with fault length faster than does the modulus, with increasing yield strength being of lesser importance. In order for larger (and deeper) faults to maintain $n=1$, all three factors (driving stress, near-tip yield strength, and modulus) must increase in such a way as to precisely maintain the D/L ratio (and $n=1$).

In order for fault displacement to scale linearly with fault length on planetary bodies with different gravities, the driving stress acting on faults of different lengths (and therefore down-dip heights) must be approximately constant. In the preceding analysis (Section 3) we assumed for consistency a uniform depth of 100 m in the calculation of driving stress for all faults. This was necessary because the expression for driving stress typically used in fault-slip calculations like these (e.g. Cowie and Scholz, 1992b; Scholz, 1997) assumes a value for normal stress, which is depth-dependent. A dependence of shear driving stress on the average normal stress resolved on the fault requires that longer and thus deeper faults have greater values of driving stress acting on them than shorter, shallower faults. From Eq. (6), having the driving stress proportional to fault length would require (a) a corresponding decrease in near-tip yield strength with increasing fault length, or (b) a decrease in modulus with fault length and, equivalently, increasing depth, assuming a constant frictional strength with depth in the crust. A decrease in modulus with depth is inconsistent with observations of modulus increase with depth (e.g. Rubin, 1990). In order for the D/L ratio to remain constant over a range of fault lengths, the numerator in Eq. (6) must increase with fault size in concert with the increase in modulus with depth (Fig. 3), although the magnitude of increase may be lessened somewhat by a possible scale-dependent reduction in modulus (Gudmundsson, 2004). Thus, longer faults either must have smaller near-tip yield strength with constant driving stress or the driving stress must decrease with constant near-tip strength. Because rock strength and modulus are known to decrease with

increasing scale (e.g. Bieniawski, 1989; Schultz, 1996), we conclude that $n=1$ scaling is consistent with approximately constant driving stress, with near-tip yield strength decreasing, and average crustal modulus increasing, as the fault size increases.

Scatter in *D-L* datasets, of perhaps a factor of 5, arises from several sources including mechanical interaction and linkage (e.g. Cowie and Scholz, 1992a; Cartwright et al., 1995; Dawers and Anders, 1995; Clark and Cox, 1996; Schultz, 1999; Gupta and Scholz, 2000b; Schultz and Fossen, 2002), which are both found on Earth and Mars (e.g. Schultz, 1997, 1999, 2000a; Schultz and Fori, 1996; Wilkins et al., 2002; Wilkins and Schultz, 2003; Polit et al., 2005a,b; Polit, 2005). Calculated variations in rock type or pore-pressure state appear small in relation to the typical scatter found in fault data sets (e.g. Clark and Cox, 1996).

4.1. Mars

Values of the main parameters for Mars, normalized by the values for the terrestrial wet basaltic rock mass, are shown in Table 2 and Figs. 4 and 5. For the same conditions of rock type (e.g. basaltic rock mass), fault type (normal), and fluid-saturated crustal rocks (i.e. 'wet' conditions), g reduces D_{max} by $g_{Mars}/g_{Earth}=0.38$ (via the driving stress term, with $g_{Mars}=3.72$ m s^{-2}; Esposito et al., 1992). Yield strength in shear scales with gravity, with the strength of the Martian basaltic rock mass being ~ 0.5 of the corresponding terrestrial one. Modulus decreases with decreasing g, to a normalized value of ~ 0.84 for the (wet) Martian case. The combined effect of g on all three key factors discussed above ($0.38\times0.5\times0.84=0.16$) is a reduction in D/L of about a factor of 5–6, consistent with the data from Martian normal faults (Fig. 1) and Martian thrust faults (Fig. 6).

4.2. Mercury

Currently, only topographic measurements of thrust faults (Fig. 6) are available for Mercury (Watters et al., 2000, 2002). The scaling relations for Mercurian thrust faults are the same as those for Martian faults in dry crustal rock, given comparable values of planetary gravity ($g_{Mercury}=3.78$ m s^{-2}; Turcotte and Schubert, 1982, p. 430). The magnitude of maximum displacement for a fault on Mercury should be about

Table 2
Comparison of parameters for normal faults on Earth and Mars

	σ_d (MPa)	σ_y (MPa)	E (GPa)	D_{max}/L	σ_y/σ_d
Earth	0.28	1.19	13.35	1.965×10^{-2}	4.27
Mars	0.11	0.613	11.27	4.075×10^{-3}	5.82
Norm	0.38	0.514	0.84	0.21	1.39

Quantities in headings are defined in Fig. 4. Values calculated using depth $z=100$ m for wet basalt (on both planets) using RMR=50, $m_i=22$, $\sigma_c=250$ MPa, dry rock density $\rho=2900$ kg m^{-3}, and deformation modulus (for wet basalt) of $E^*=10$ GPa. Normalized values (third row, 'Norm') are Mars/Earth.
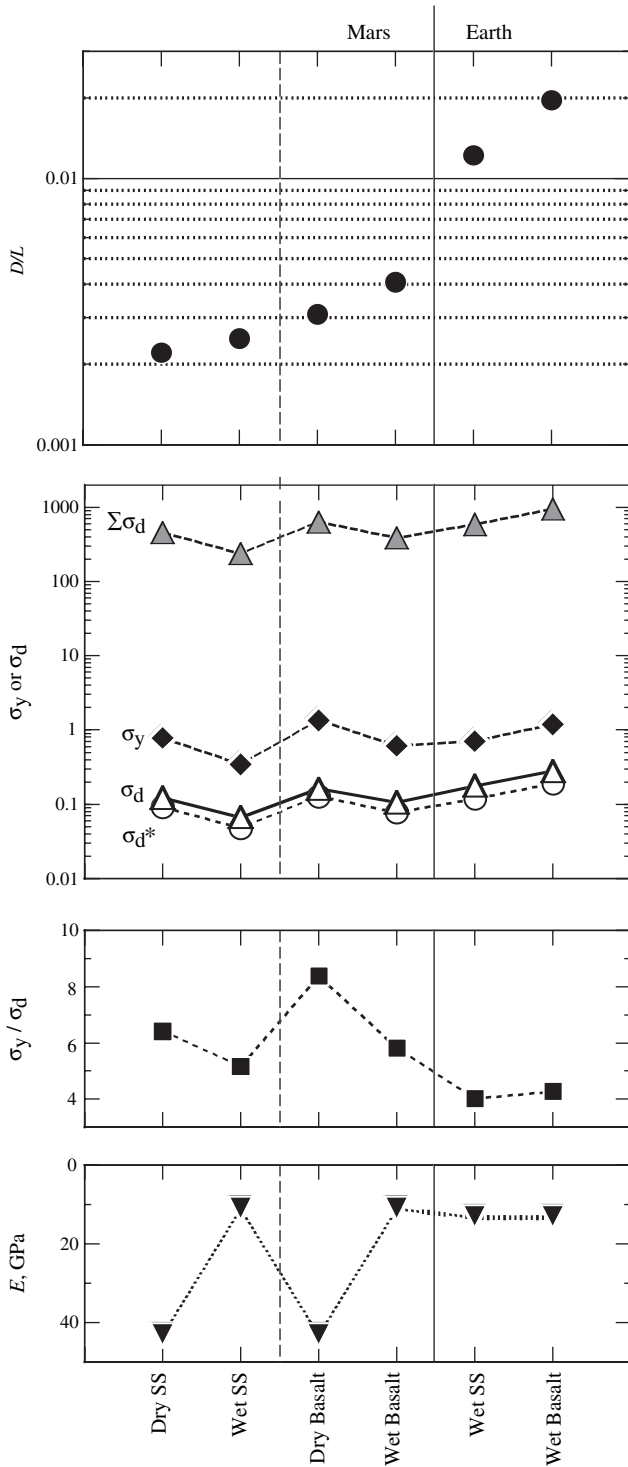
Fig. 4. Effect of gravity on key parameters for two lithologies (sandstone (SS) and basaltic) and two pore-water conditions (saturated and dry). Upper panel, D/L ratio; second panel, shear yield strength (σ_y), shear driving stress (σ_d), and cumulative shear driving stress ($\Sigma\sigma_d$); third panel, yield strength/driving stress ratio; lowest panel, Young's modulus. All values except D/L are averages over 100-m depth interval.

16% of a comparable fault on Earth (Fig. 5, upper panel; Fig. 7).

The normal fault data discussed for Mars above were fit with $L/H = 3$ and $N = 3000$. However, the scaling relations using
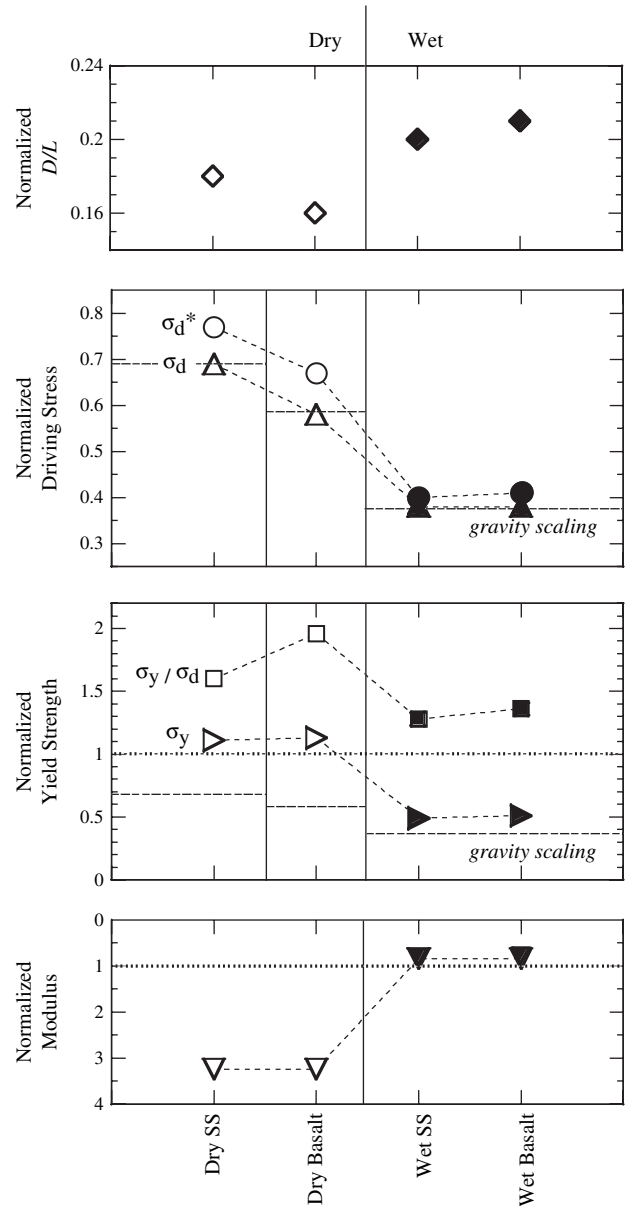
Fig. 5. Values of key parameters (shown in Fig. 4) normalized by values for wet terrestrial basaltic rock mass. Dashed horizontal lines show pure gravity scaling (g_{planet}/g_{Earth}) of each parameter. Symbols and labels as in Fig. 4.

these values of fault aspect ratio and N overpredict the displacements on Martian and Mercurian thrust faults, regardless of lithology and crustal water content (see Fig. 6), by about a factor of 5, with a predicted value of $D/L \sim 10^{-2}$. We interpret this discrepancy as an indication that the aspect ratios of the terrestrial and planetary thrust faults in our dataset are not equal.

Datasets for terrestrial thrust faults (Fig. 6) include faults within a fold-and-thrust belt from (a) a thin-skinned fold-and-thrust belt within sedimentary rocks (data from the Canadian Rocky Mountains; Elliott, 1976); (b) the Yakima fold belt in basaltic rocks (Washington State; Mége and Riedel, 2001); (c) the Puente Hills blind thrust fault system
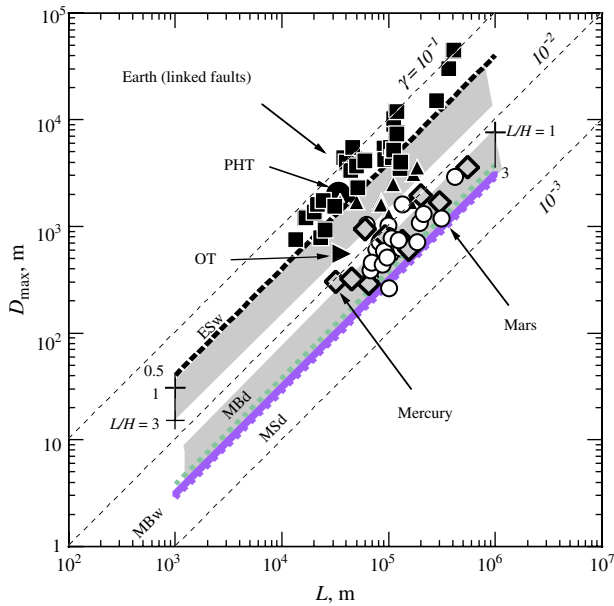
Fig. 6. *D-L* data for thrust faults from Earth (black squares and triangles), Mars (open circles) and Mercury (gray diamonds); data from Elliott (1976), black squares; Mége and Riedel (2001), black triangles; Shaw et al. (2002), black circle (Puente Hills Blind-Thrust System, 'PHT'); Davis et al. (2005), right-pointing black triangle (Ostler Thrust, 'OT'); Watters et al. (2000, 2002) and Watters (2003). Calculated scaling relations labeled as in Fig. 1 but with *L/H*=0.5 for terrestrial thrust faults with lower ticks at *L/H*=1.0 and 3.0 (upper shaded region in the figure), and *L/H*=3.0 for Martian and Mercurian thrust faults with upper tick at *L/H*=1.0 (lower shaded region).

in the transform plate margin of southern California; and (d) mechanically interacting fault segments propagating upward through unconsolidated alluvium (data from the Ostler fault zone, New Zealand; Davis et al., 2005). The data for thrust
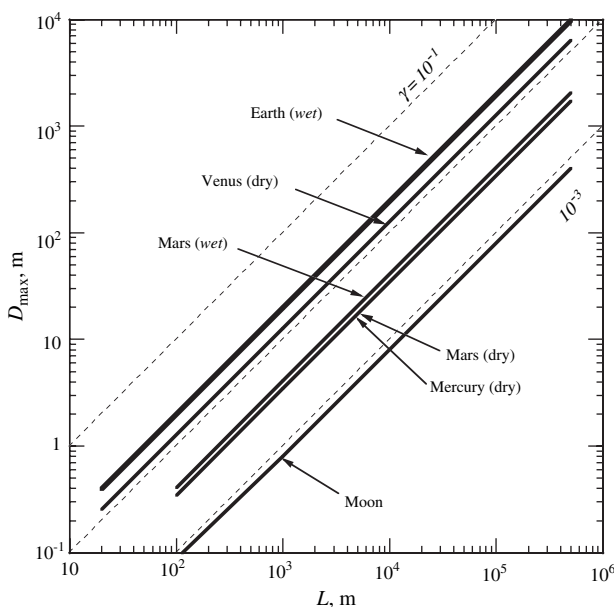

Fig. 7. Predicted values of *D/L* for smaller planets and satellites. All curves calculated for normal faults assuming *L/H*=3, *N*=3000, and basaltic rock mass parameters.

faults that cut anticlines in the Yakima fold-and-thrust belt suggest either larger aspect ratios consistent with restriction of the faults to near-surface (basaltic) units or uncompensated dissipation of fault displacement into folding of the basalts (see Davis et al. (2005) for methods to compare fold- and fault-related deformation). Displacements along the composite Puente Hills fault array are consistent with those from the Canadian Rockies. The cumulative displacement value for the composite Ostler, New Zealand, fault zone is consistent with those from the Yakima fold belt (Fig. 6); the displacement values for individual segments from the Ostler fault zone are influenced by (a) their strong mechanical interaction ('soft-linkage') with adjacent segments and (b) smaller modulus of the faulted unconsolidated alluvium, and substantially reduced by offset of younger strata that do not span the full duration of faulting (Davis et al., 2005), leading to smaller *D/L* values for the segments than for the entire fault zone.

Seismic profiling of the Puente Hills thrust fault array suggests that individual fault segments are 'tall' (Shaw et al., 2002), with aspect ratios (*L/H*) in the range of 2–3; the composite, soft-linked fault array appears to have *L ~ H*. Although the depth of faulting along the Ostler thrust fault array is uncertain (Davis et al., 2005), the authors' data imply that *L > H* for this array. Aspect ratios of *L/H* < 1 ('tall faults') are used here (Fig. 6) in an attempt to better represent the likely down-dip shapes of the terrestrial thrust faults from Elliott's (1976), Mége and Riedel's (2001), and Shaw et al.'s (2002) datasets from fold-and-thrust belts that may sole downward into basal décollements (e.g. Davison, 1994). Using *L/H*=0.5, the terrestrial thrust fault data are fit with *N*=1000 (Fig. 6); using *L/H*=3 with *N*=1000 produces acceptable fits to the planetary thrust fault data (Fig. 6) as well as to the Ostler thrust fault array in New Zealand. We infer that many Martian and Mercurian thrust faults may have aspect ratios greater than one (e.g. Nicol et al., 1996; shaded area on Fig. 6), whereas many of the terrestrial thrust faults (especially those in the Canadian Rockies) have aspect ratios less than one (heavy dashed line on Fig. 6). However, additional measurements of displacement, length, and height for thick-skinned terrestrial thrust faults located outside of a plate margin, especially surface-breaking examples, would permit more robust evaluation of *D-L* scaling of surface-breaking thrust faults on other planetary bodies.

4.3. Moon

Values of fault displacement on the Moon, sufficiently accurate for *D-L* scaling relations to be well defined, are not available given the coarse horizontal resolution of the available topography (30 km by 30 km grid; Zuber et al., 1994), since structural topography along narrow faults (≪30 km wide) is diluted by nondeformed terrain that comprises most of the remainder of the grid cell. We can predict the values of the *D/L* ratio that would be expected for lunar faults using the approach in this paper. Letting *g*=1.6 m s^{-2} (Vaniman et al., 1991) and assuming dry (anhydrous) average rock

density (using anorthosite; e.g. Taylor et al., 1991) of 2750 kg m^{-3} (Turcotte and Schubert, 1982, p. 432), comparable with that of granodiorite, we find that the *D/L* ratio of lunar faults should be approximately 0.04 that of terrestrial faults (Figs. 7 and 8). As a result, the throws on lunar normal faults, and on the thrust faults beneath lunar wrinkle ridges, should be quite small: only 4% of what a terrestrial fault of similar size would produce.

5. Conclusions

The systematically smaller values of displacement for faults on Mars and Mercury result from the reduced surface gravitational acceleration of these planets relative to that of the Earth. The *D-L* scaling of Martian faults depends on the water content of the crust, with faults in wet crust generating 33% larger displacements than those in dry crust, primarily through the smaller value of modulus for wet crustal rock (despite somewhat weaker yield strength for wet conditions). *D-L* scaling of thrust faults on Mercury and Mars is consistent with aspect ratios (length/height) of 1−3, suggesting that these faults are 'long' and not linked down-dip to décollements as are examples of thrust faults from the transform plate margin in southern California and the Canadian Rockies fold-and-thrust belt, which apparently function as tall segmented faults

with smaller aspect ratios (*L/H*<1). Further, the differences in strain with the type of fault−fold coupling (i.e. fault−bend, fault−propagation, and faulted detachment folds) require further investigation and quantification. Collection of displacement-length and down-dip height data from terrestrial thrust faults, located both within fold-and-thrust belts and in continental interiors (i.e. both thin- and thick-skinned settings and accounting for progressive segment linkage and associated displacement transfer), is critical for testing the possible roles of fault shape and down-dip linkage on the scaling relations for thrust faults from Earth and elsewhere.

Assessment of *D-L* scaling relations of faults on the Moon, Venus, and icy satellites of the outer solar system is currently hindered by large uncertainties in displacement (due to low-resolution, or unavailable, topographic data) and, to a lesser extent, length (due to low-resolution imaging data). We infer from our analysis that faults on Venus should accumulate somewhat smaller displacements than their terrestrial counterparts given a ~10% reduction in gravity (g=8.8 m s^{-2}) relative to the Earth. Faults on the icy satellites of Jupiter and Saturn probably also scale with gravity, with particular values of the *D/L* ratio depending on appropriate values of near-tip ice strength and ice stiffness. Because brittle strains depend on the *D/L* ratio (along with the fault density; Gupta and Scholz, 2000b; Schultz, 2003), the average strain accommodated by faulting at the surface of a planetary body, for the same style of tectonic domain, should generally decrease as a function of gravity.

By implication, other types of structures such as joints (e.g. Vermilye and Scholz, 1995), dikes (Schultz et al., 2004), and deformation bands (e.g. Fossen and Hesthammer, 1997; Schultz and Fossen, 2002; Schultz and Siddharthan, 2005) that form on other planets and satellites should also scale in *D/L* with gravity. This is because the same physical factors of driving stress, rock yield strength, and modulus that regulate fault scaling also influence the growth and displacement of these structures.

Fig. 8. Summary of *D-L* scaling for terrestrial planets calculated for wet basaltic crusts (dashed curves) and dry basaltic crusts (solid curves). Lower panel, values for smaller planets normalized by (wet) terrestrial ones.

References

Bieniawski, Z.T., 1989. Engineering Rock Mass Classifications: a Complete Manual for Engineers and Geologists in Mining, Civil, and Petroleum Engineering. Wiley, New York.

Bolt, B.A., 1988. Earthquakes. Freeman, New York.

Brace, W.F., Kohlstedt, D.L., 1980. Limits on lithospheric stress imposed by laboratory experiments. Journal of Geophysical Research 85, 6248−6252.

Bürgmann, R., Pollard, D.D., Martel, S.J., 1994. Slip distributions on faults: effects of stress gradients, inelastic deformation, heterogeneous host-rock
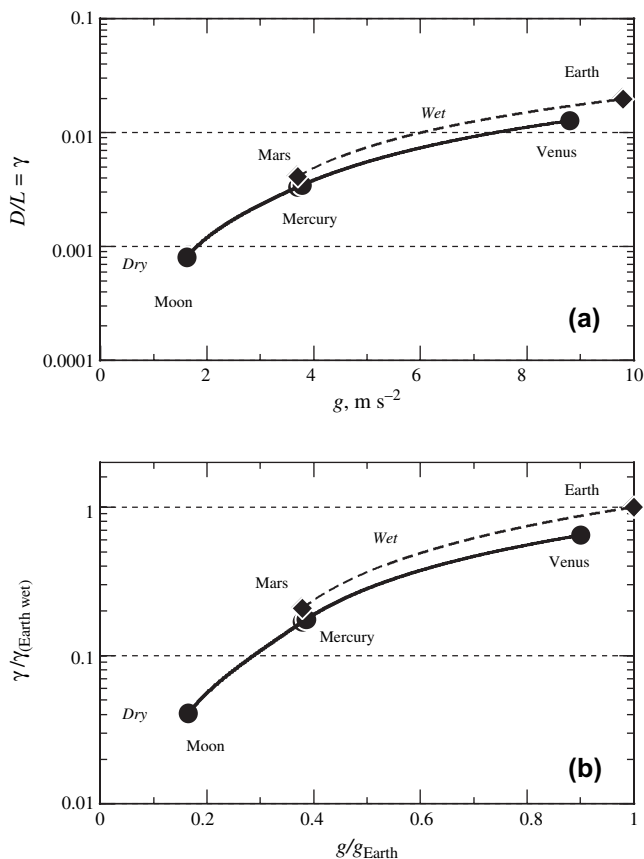
stiffness, and fault interaction. Journal of Structural Geology 16, 1675–1690.

Cartwright, J.A., Trudgill, B.D., Mansfield, C.S., 1995. Fault growth by segment linkage: an explanation for scatter in maximum displacement and trace length data from the Canyonlands Grabens of SE Utah. Journal of Structural Geology 17, 1319–1326.

Clark, R.M., Cox, S.J.D., 1996. A modern regression approach to determining fault displacement-length relationships. Journal of Structural Geology 18, 147–152.

Cooke, M.L., 1997. Fracture localization along faults with spatially varying friction. Journal of Geophysical Research 102, 22425–22434.

Cowie, P.A., Scholz, C.H., 1992. Displacement-length scaling relationships for faults: data synthesis and discussion. Journal of Structural Geology 14, 1149–1156.

Cowie, P.A., Scholz, C.H., 1992. Physical explanation for the displacement-length relationship of faults using a post-yield fracture mechanics model. Journal of Structural Geology 14, 1133–1148.

Cowie, P.A., Shipton, Z.K., 1998. Fault tip displacement gradients and process zone dimensions. Journal of Structural Geology 20, 983–997.

Davis, K., Burbank, D.W., Fisher, D., Wallace, S., Nobes, D., 2005. Thrust-fault growth and segment linkage in the active Ostler fault zone, New Zealand. Journal of Structural Geology 27, 1528–1546.

Davis, P.A., Golombek, M.P., 1990. Discontinuities in the shallow Martian crust at Lunae, Syria, and Sinai Plana. Journal of Geophysical Research 95, 14231–14248.

Davison, I., 1994. Linked fault systems; extensional, strike-slip and contractional. In: Hancock, P.L. (Ed.), Continental Deformation. Pergamon, New York, pp. 121–142.

Dawers, N.H., Anders, M.H., 1995. Displacement-length scaling and fault linkage. Journal of Structural Geology 17, 607–614.

Dawers, N.H., Anders, M.H., Scholz, C.H., 1993. Growth of normal faults: displacement-length scaling. Geology 21, 1107–1110.

Elliott, D., 1976. The energy balance and deformation mechanism of thrust sheets. Philosophical Transactions of the Royal Society of London A283, 289–312.

Esposito, P.B., Banerdt, W.B., Lindal, G.F., Sjogren, W.L., Slade, M.A., Bills, B.G., Smith, D.E., Balmino, G., 1992. Gravity and topography. In: Kieffer, H.H., Jakosky, B.M., Snyder, C.W., Matthews, M.S. (Eds.), Mars. University of Arizona Press, Tucson, pp. 209–248.

Fossen, H., Hesthammer, J., 1997. Geometric analysis and scaling relations of deformation bands in porous sandstone. Journal of Structural Geology 19, 1479–1493.

Gudmundsson, A., 2004. Effects of Young's modulus on fault displacement. Comptes Rendus de Geoscience 336, 85–92.

Gupta, A., Scholz, C.H., 2000. A model of normal fault interaction based on observations and theory. Journal of Structural Geology 22, 865–879.

Gupta, A., Scholz, C.H., 2000. Brittle strain regime transition in the Afar depression: implications for fault growth and seafloor spreading. Geology 28, 1078–1090.

Hauber, E., Kronberg, P., 2005. The large Thaumasia graben on Mars: is it a rift? Journal of Geophysical Research 110, E07003, doi:10.1029/2005JE002407.

Hoek, E., Brown, E.T., 1980. Empirical strength criterion for rock masses. Journal of the Geotechnical Engineering Division, American Society of Civil Engineers 106, 1013–1035.

Jaeger, J.C., Cook, N.G.W., 1979. Fundamentals of Rock Mechanics, 3rd ed. Chapman and Hall, New York. 593pp.

Manighetti, I., King, G.C.P., Gaudemer, Y., Scholz, C.H., Doubre, C., 2001. Slip accumulation and lateral propagation of active normal faults in Afar. Journal of Geophysical Research 106, 13667–13696.

Marone, C., 1998. Laboratory-derived friction laws and their application to seismic faulting. Annual Review of Earth and Planetary Sciences 26, 643–696.

Martel, S.J., 1997. Effects of cohesive zones on small faults and implications for secondary fracturing and fault trace geometry. Journal of Structural Geology 19, 835–847.

Martel, S.J., 1999. Mechanical controls on fault geometry. Journal of Structural Geology 21, 585–596.

McGarr, A., Gay, N.C., 1978. State of stress in the Earth's crust. Annual Reviews of Earth and Planetary Science 6, 405–436.

Mége, D., Riedel, S.P., 2001. A method for estimating 2D wrinkle ridge strain from application of fault displacement scaling to the Yakima folds, Washington. Geophysical Research Letters 28, 3545–3548.

Moore, J.M., Schultz, R.A., 1999. Processes of faulting in jointed rocks of Canyonlands National Park, Utah. Geological Society of America Bulletin 111, 808–822.

Neuffer, D.P., Schultz, R.A., in press. Mechanisms of slope failure in Valles Marineris, Mars. Quarterly Journal of Engineering Geology and Hydrogeology.

Nicol, A., Watterson, J., Walsh, J.J., Childs, C., 1996. The shapes, major axis orientations and displacement patterns of fault surfaces. Journal of Structural Geology 18, 235–248.

Okubo, C.H., Schultz, R.A., 2004. Mechanical stratigraphy in the western equatorial region of Mars based on thrust fault-related fold topography and implications for near-surface volatile reservoirs. Geological Society of America Bulletin 116, 594–605.

Okubo, C.H., Schultz, R.A., 2006. Variability in Early Amazonian Tharsis stress state based on wrinkle ridges and strike-slip faulting. Journal of Structural Geology 28, 2169–2181.

Polit, A.T., 2005. Influence of mechanical stratigraphy and strain on the displacement-length scaling of normal faults on Mars. Unpublished M.S. thesis, University of Nevada, Reno.

Polit, A.T., Schultz, R.A., Soliva, R., 2005. A tale of two stratigraphies: from Alba Patera to the northern plains (abstract). In: Lunar and Planetary Science XXXVI (on CD-ROM).

Polit, A.T., Schultz, R.A., Soliva, R., 2005. Influence of mechanical stratigraphy and strain on the displacement-length scaling of normal faults from Alba Patera to the northern plains, Mars (abstract). Eos (Transactions, American Geophysical Union) 86 (supplement), P51B-0921.

Pollard, D.D., Segall, P., 1987. Theoretical displacements and stresses near fractures in rock: with applications to faults, joints, veins, dikes, and solution surfaces. In: Atkinson, B.K. (Ed.), Fracture Mechanics of Rock. Academic Press, London, pp. 277–349.

Rubin, A.M., 1990. A comparison of rift-zone tectonics in Iceland and Hawaii. Bulletin of Volcanology 52, 302–319.

Schlische, R.W., Young, S.S., Ackerman, R.V., Gupta, A., 1996. Geometry and scaling relations of a population of very small rift related normal faults. Geology 24, 683–686.

Scholz, C.H., 1997. Earthquake and fault populations and the calculation of brittle strain. Geowissenschaften 15, 124–130.

Scholz, C.H., 1998. Earthquakes and friction laws. Nature 391, 37–42.

Scholz, C.H., 2002. The Mechanics of Earthquakes and Faulting, 2nd ed. Cambridge University Press. 471pp.

Schultz, R.A., 1989. Strike-slip faulting of ridged plains near Valles Marineris, Mars. Nature 341, 424–426.

Schultz, R.A., 1996. Relative scale and the strength and deformability of rock masses. Journal of Structural Geology 18, 1139–1149.

Schultz, R.A., 1997. Displacement-length scaling for terrestrial and Martian faults: implications for Valles Marineris and shallow planetary grabens. Journal of Geophysical Research 102, 12009–12015.

Schultz, R.A., 1999. Understanding the process of faulting: selected challenges and opportunities at the edge of the 21st century. Journal of Structural Geology 21, 985–993.

Schultz, R.A., 2000a. Fault-population statistics at the Valles Marineris Extensional Province, Mars: implications for segment linkage, crustal strains, and its geodynamical development. Tectonophysics 316, 169–193.

Schultz, R.A., 2000b. Localization of bedding plane slip and backthrust faults above blind thrust faults: keys to wrinkle ridge structure. Journal of Geophysical Research 105, 12,035–12,052.

Schultz, R.A., 2003. A method to relate initial elastic stress to fault population strains. Geophysical Research Letters 30, 1593, doi:10.1029/2002GL016681.

Schultz, R.A., Fori, A.N., 1996. Fault-length statistics and implications of graben sets at Candor Mensa, Mars. Journal of Structural Geology 18, 373–383.

Schultz, R.A., Fossen, H., 2002. Displacement-length scaling in three dimensions: the importance of aspect ratio and application to deformation bands. Journal of Structural Geology 24, 1389–1411.

Schultz, R.A., Lin, J., 2001. Three-dimensional normal faulting models of Valles Marineris, Mars, and geodynamic implications. Journal of Geophysical Research 106, 16549–16566.

Schultz, R.A., Siddharthan, R., 2005. A general framework for the occurrence and faulting of deformation bands in porous granular rocks. Tectonophysics 411, 1–18.

Schultz, R.A., Soliva, R., 2005. Rate-and-state friction and linear fault displacement profiles. Eos (Transactions, American Geophysical Union), 86, supplement, T14B–01.

Schultz, R.A., Watters, T.R., 2001. Forward mechanical modeling of the Amenthes Rupes thrust fault on Mars. Geophysical Research Letters 28, 4659–4662.

Schultz, R.A., Okubo, C.H., Goudy, C.L., Wilkins, S.J., 2004. Igneous dikes on Mars revealed by MOLA topography. Geology 32, 889–892.

Shaw, J.H., Plesch, A., Dolan, J.F., Pratt, T.L., Fiore, P., 2002. Puente Hills blind-thrust system, Los Angeles, California. Seismological Society of America Bulletin 92, 2946–2960.

Soliva, R., Benedicto, A., 2004. A linkage criterion for segmented normal faults. Journal of Structural Geology 26, 2251–2267.

Soliva, R., Schultz, R.A., Benedicto, A., 2005. Three-dimensional displacement-length scaling and maximum dimension of normal faults in layered rocks. Geophysical Research Letters 32, L16302, doi:10.1029/2005GL023007.

Soliva, R., Benedicto, A., Maerten, L., 2006. Spacing and linkage of confined normal faults: importance of mechanical thickness. Journal of Geophysical Research 110, B01402, doi:10.1029/2004JB003507.

Taylor, G.J., Warren, P., Ryder, G., Delano, J., Pieters, C., Lofgren, G., 1991. Lunar rocks. In: Heiken, G.H., Vaniman, D.T., French, B.M. (Eds.), Lunar Sourcebook. Cambridge University Press, Cambridge, pp. 183–284.

Turcotte, D.L., Schubert, G., 1982. Geodynamics. Wiley, New York.

Vaniman, D., Reedy, R., Heiken, G., Olhoeft, G., Mendell, W., 1991. The lunar environment. In: Heiken, G.H., Vaniman, D.T., French, B.M. (Eds.), Lunar Sourcebook. Cambridge University Press, Cambridge, pp. 27–60.

Vermilye, J.M., Scholz, C.H., 1995. Relation between vein length and aperture. Journal of Structural Geology 17, 423–434.

Watters, T.R., 2003. Thrust faults along the dichotomy boundary in the eastern hemisphere of Mars. Journal of Geophysical Research 108, 5054, doi:10.1029/2002JE001934.

Watters, T.R., Robinson, M.S., Cook, A.C., 1998. Topography of lobate scarps on Mercury: new constraints on the planet's contraction. Geology 26, 991–994.

Watters, T.R., Schultz, R.A., Robinson, M.S., 2000. Displacement-length scaling relations of thrust faults associated with lobate scarps on Mercury and Mars: comparison with terrestrial faults. Geophysical Research Letters 27, 3659–3662.

Watters, T.R., Schultz, R.A., Robinson, M.S., Cook, A.C., 2002. The mechanical and thermal structure of Mercury's early lithosphere. Geophysical Research Letters 29 (11), 37.1–37.4.

Wibberley, C.A.J., Petit, J.-P., Rives, T., 1999. Mechanics of high displacement gradient faulting prior to lithification. Journal of Structural Geology 21, 251–257.

Wibberley, C.A.J., Petit, J.-P., Rives, T., 2000. Mechanics of cataclastic 'deformation band' faulting in high-porosity sandstone, Provence. Earth and Planetary Sciences 331, 419–425.

Wilkins, S.J., Gross, M.R., 2002. Normal fault growth in layered rocks at Split Mountain, Utah: influence of mechanical stratigraphy on dip linkage, fault restriction and fault scaling. Journal of Structural Geology 24, 1413–1429 (erratum, Journal of Structural Geology 24, 2007).

Wilkins, S.J., Schultz, R.A., 2003. Cross faults in extensional settings: stress triggering, displacement localization, and implications for the origin of blunt troughs in Valles Marineris, Mars. Journal of Geophysical Research 108, 5056, doi:10.1029/2002JE001968.

Wilkins, S.J., Schultz, R.A., 2005. 3D cohesive end-zone model for source scaling of strike-slip interplate earthquakes. Seismological Society of America Bulletin 95, 2232–2258.

Wilkins, S.J., Schultz, R.A., Anderson, R.C., Dohm, J.M., Dawers, N.C., 2002. Deformation rates from faulting at the Tempe Terra extensional province, Mars. Geophysical Research Letters 29, 1884, doi:10.1029/2002GL015391.

Willemse, E.J.M., 1997. Segmented normal faults: correspondence between three-dimensional mechanical models and field data. Journal of Geophysical Research 102, 675–692.

Willemse, E.J.M., Pollard, D.D., 1998. On the orientation and pattern of wing cracks and solution surfaces at the tips of a sliding flaw or fault. Journal of Geophysical Research 103, 2427–2438.

Willemse, E.J.M., Pollard, D.D., Aydin, A., 1996. Three-dimensional analyses of slip distributions on normal fault arrays with consequences for fault scaling. Journal of Structural Geology 18, 295–309.

Zoback, M.D., Barton, C.A., Brudy, M., Castillo, D.A., Finkbeiner, T., Grollimund, B.R., Moos, D.B., Peska, P., Ward, C.D., Wiprut, D.J., 2003. Determination of stress orientation and magnitude in deep wells. International Journal of Rock Mechanics and Mining Sciences 40, 1049–1076.

Zuber, M.T., Smith, D.E., Lemoine, F.G., Neumann, G.A., 1994. The shape and internal structure of the Moon from the Clementine mission. Science 266, 1839–1843.